Biosensors and Bioelectronics 25 (2010) 2329–2335

Contents lists available at ScienceDirect

Biosensors and Bioelectronics

journal homepage: www.elsevier.com/locate/bios

An electrochemical acetylcholine biosensor based on nanoshells of hollow nickel microspheres-carbon microparticles-Nafion nanocomposite

N. Sattarahmady[a], H. Heli[b,c,*], A.A. Moosavi-Movahedi[d]

[a] Department of Biochemistry, Shiraz University of Medical Sciences, Shiraz, Iran
[b] Laboratory of Analytical and Physical Electrochemistry, Department of Chemistry, Islamic Azad University, Fars Science and Research Branch, P.O. Box 73715-181, Marvdasht, Iran
[c] Young Researchers Club, Islamic Azad University, Fars Science and Research Branch, Marvdasht, Iran
[d] Institute of Biochemistry and Biophysics, University of Tehran, Tehran, Iran

ARTICLE INFO

Article history:
Received 16 January 2010
Received in revised form 22 March 2010
Accepted 23 March 2010
Available online 1 April 2010

Keywords:
Acetylcholine
Nickel
Nanoshell
Electrocatalysis
Nanobiosensor
Nanocomposite

ABSTRACT

Electrocatalytic oxidation of acetylcholine (ACh) on different nickel-based composites was investigated. Cyclic voltammetry, steady-state polarization measurements and chronoamperometry were employed to study the mechanism and kinetics of the oxidation process. The results showed that ACh was irreversibly oxidized on nickel nanoshells-carbon microparticles-Nafion nanocomposite with an excellent catalytic activity. The catalytic rate constant and the transfer coefficient for the electrocatalytic oxidation of ACh and the diffusion coefficient of ACh were obtained using cyclic voltammetry, steady-state polarization measurements and chronoamperometry. A sensitive and time-saving hydrodynamic amperometry method was developed for the determination of ACh. The nanocomposite showed a high sensing performance with a sensitivity of $48.58 \pm 0.52\,mA\,M^{-1}\,cm^{-2}$ and a limit of detection of 49.33 nM. The nanocomposite represented many advantages as an ACh biosensor such as simple preparation method without using any specific enzyme or reagent, excellent catalytic activity, high sensitivity, long-term stability, and antifouling property toward ACh and its oxidation product(s). Sensitivity and detection limit of the present biosensor are better than all of the reports appeared in the literature.

1. Introduction

Acetylcholine (ACh) is the earliest discovered neurotransmitter which has an important function in the cholinergic system where it acts as a transmitter of impulses on the cholinergic synapses. It can be found in the central nervous system, neuromuscular junctions, spinal cord, and preganglionic and motor neurons. ACh affects learning, memory and muscle tones (John and Carolina, 2001). Various neuropsychological and neuropsychiatric disorders such as Alzheimer's disease, Parkinson's disease, progressive dementia and schizophrenia may occur due to accumulation of acetylcholine in nervous tissue when it is not metabolized (Davis and Berger, 1979). These facts have made a considerable interest to the in vitro and in vivo determination of ACh as an integral part of cholinergic research (Pepeu and Giovannini, 2004).

Unfortunately, ACh is neither easily oxidizable/reducible nor possesses structural characteristics (electroreactive, chromophore or fluorophore groups) allowing a sensitive detection using electrochemical, spectrophotometric or fluorometric methods. Therefore, well established methods typically used for other neurotransmitters are useless and the majority of the methods developed for its determination generally require a conversion into more easily detectable compounds. Several methods for ACh detection have been reported including enzyme-based biosensors (Burmeister et al., 2008), potentiometry using an ion-selective electrode (Barsoum et al., 2004), radioimmunoassay (Woodman et al., 1982), and gas chromatography-mass spectrometry and liquid chromatography coupled to post-column enzymatic detection (Tsai, 2000). However, the enzyme-based methods are expensive and suffer from insufficient stability and loss of enzyme activity during immobilization process. The method of potentiometry lacks sensitivity and specificity. The other methods are complicated, time-consuming and require expensive equipment that was not available to many investigators. In this regards, developments of electrochemical non-enzymatic ACh biosensors have received continuous interest (Shibli and Beenakumari, 2006; Shibli et al., 2006; Lin and Chou, 2005; Heli et al., 2009a). Electrochemical non-enzymatic ACh biosensors can represent sensitive, selective, and the prevention

* Corresponding author at: Laboratory of Analytical and Physical Electrochemistry, Department of Chemistry, Islamic Azad University, Fars Science and Research Branch, P.O. Box 73715-181, Marvdasht, Iran. Tel.: +98 728 46 92 114; fax: +98 728 46 92 153.
E-mail address: hheli7@yahoo.com (H. Heli).

0956-5663/$ – see front matter © 2010 Elsevier B.V. All rights reserved.
doi:10.1016/j.bios.2010.03.031

of fouling by adsorbed intermediates and some anions (Heli et al., 2009a). These advantages lie in the properties of the electrode materials.

Hollow structures have attracted much research attention in recent years due to interesting properties that differ from their solid counterparts and their potential applications in drug storage and release, catalysis, separation, chromatography, lightweight materials, and optical, electronic, magnetic, catalytic, acoustic and sensing devices (Lou et al., 2008). These potential applications arise from low density, large specific area, mechanical and thermal stability, and surface permeability.

In the present work, the electrocatalytic oxidation of ACh on the surface of a hollow nickel microspheres-carbon microparticles-Nafion has been investigated.

2. Experimental

Nickel microparticles with the diameter of <10 μm were obtained from Sima Felez, Co., Iran. Zinc powder was purchased from Merck. Graphite fine powder (denoted as carbon microparticles) with a particle size of <50 μm was obtained from Merck. All other chemicals used in the experiments were of analytical grade from Merck or Sigma and were used without further purification. All solutions were prepared with doubly distilled water.

Nanoshells of hollow nickel microspheres were synthesized using sacrificial-core technique (Ning et al., 2005) via a galvanic replacement reaction. In a typical experiment, 0.50 g zinc powder was first dispersed into 5 mL acetone and 100 mL distilled water by ultrasonication for 10 min. In another beaker, 3.0 g $NiCl_2{\cdot}2H_2O$ was dissolved in 50 mL distilled water and 20 mL 25% (v/v) concentrated ammonia solution was added until a blue coordination compound solution was obtained. Then the nickel–ammonia complex solution was added dropwise into the first-prepared suspended mixture of zinc powder. The galvanic replacement of nickel with zinc was carried out for 10 h under stirring. A solid product was then precipitated. The obtained black products were treated with 20 mL 11.0 M NaOH solution for 6 h. The black product obtained was then washed with distilled water and alcohol, respectively.

Nickel nanoparticles were synthesized by a polyol method in the presence of a capping agent (Jin et al., 2006). Typically, a given amount of $Ni(NO_3)_2{\cdot}6H_2O$ with 1% polyvinylpyrrolidone (PVP) was dissolved in distilled water. Then 1.0 M NaOH solution was added to adjust the solution pH to 11. The mixed solution was stirred at 60 °C for 2 h. Then, the resultant $Ni(OH)_2$ slurry was filtered with a fritted glass funnel. The obtained $Ni(OH)_2$, 3.0 g NaOH, 0.4 g PVP, and 100 mL ethylene glycol were added to a three-necked flask. The mixture was stirred to form a $Ni(OH)_2$ slurry, and then refluxed at 180 °C for 4 h, filtered and finally, washed with distilled water and ethanol. The resultant product was dried at ambient temperature. Gray to black nickel nanoparticles was obtained.

Electrochemical studies were carried out in a cell containing 100 mM NaOH solution as the running electrolyte, powered by an Autolab/PGSTAT 302 N (The Netherlands). The system was run by a PC through the GPES 4.9 software. An Ag/AgCl and a platinum plate were used as the reference and counter electrodes, respectively. The working electrode was an unmodified carbon paste electrode (u-CPE) or composite electrodes.

Scanning electron microscopy (SEM) was carried out using a X-30 Philips instrument.

u-CPE was prepared by hand-mixing carbon microparticles and mineral oil with a 80/20% (w/w) ratio. The paste was packed firmly into a cavity (2 mm diameter) at the end of a Teflon tube. Electrical contact was established by a copper wire.

The composite electrodes used in this work and the corresponding abbreviations are listed in Table 1. m-Ni-CC, n-Ni-CC, Zn@Ni-CC and ns-Ni-CC were prepared by mixing carbon microparticles, mineral oil, and the respective modifiers with ratios of 60:20:20 by wt%. ns-Ni-CC-Nf was prepared by mixing carbon microparticles, mineral oil and nickel microspheres with the same ratio, and then 120 μL of a 1% (w/v) low aliphatic alcohols Nafion solution was added to (0.5 g of) the paste. ns-Ni-CC/Nf was prepared by mixing carbon microparticles, mineral oil and nickel microspheres with ratios of 60:20:20 by wt%, and then the resultant composite was covered with 10 μL of a 2% (w/v) low aliphatic alcohols Nafion solution. Therefore, Nafion was present in the bulk of ns-Ni-CC-Nf and as a covering membrane on the surface of ns-Ni-CC/Nf.

Table 1
The different working electrodes used in this work, the corresponding abbreviations and the values of catalytic efficiencies (CEs) toward the electrooxidation of ACh.

Working electrode	Abbreviation	CE
Unmodified carbon paste electrode	u-CPE	–
Nickel microparticles-carbon microparticles composite	m-Ni-CC	0.08
Nickel nanoparticles-carbon microparticles nanocomposite	n-Ni-CC	0.11
Zink core-nickel shell microparticles-carbon microparticles composite	Zn@Ni-CC	0.14
Nickel nanoshell-carbon microparticles nanocomposite	ns-Ni-CC	0.17
Nickel nanoshell-carbon microparticles-Nafion nanocomposite	ns-Ni-CC-Nf	0.27
Nickel nanoshell-carbon microparticles nanocomposite coated with Nafion solution	ns-Ni-CC/Nf	0.82

All composite electrodes, after preparation and before performing any experiment, were transferred to the supporting electrolyte and 25 potential cycles were applied in a regime of cyclic voltammetry in the potential range of 200–750 mV at a potential sweep rate of 100 mV s^{-1}.

In order to compare the catalytic efficiency of different composites toward the electrooxidation of ACh, the generated anodic currents were normalized with respect to the effective surface area and the currents in the voltammograms were reported as current densities. To obtain such effective surface areas, the anodic charge passed for the oxidation of nickel species was measured in alkaline solution for the composites; these values were related directly to the effective surface areas.

All measurements were carried out at room temperature.

3. Results and discussion

3.1. Electron microscopy

A SEM micrograph of hollow nickel microspheres was measured (see Supplementary material S1). The image showed nanoshell-mirospheres of a mean diameter of ≈6 μm which contained broken regions and cavities confirming the hollow structure of the spheres.

3.2. Study of the charge-transfer kinetics across the ns-Ni-CC/Nf/solution interface

Fig. 1A shows cyclic voltammograms of ns-Ni-CC/Nf in 100 mM NaOH solution recorded at a wide range of potential sweep rates from 7 to 3000 mV s^{-1}. A pair of well-defined peak with a mid-peak potential of 538 mV appeared in the voltammograms, and the peak-to-peak potential separation (at the potential sweep rate of 10 mV s^{-1}) was 190 mV. The voltammograms are similar to those previously reported (Hajjizadeh et al., 2008), and the involved redox transition is attributed to the presence of Ni(II)/Ni(III) species

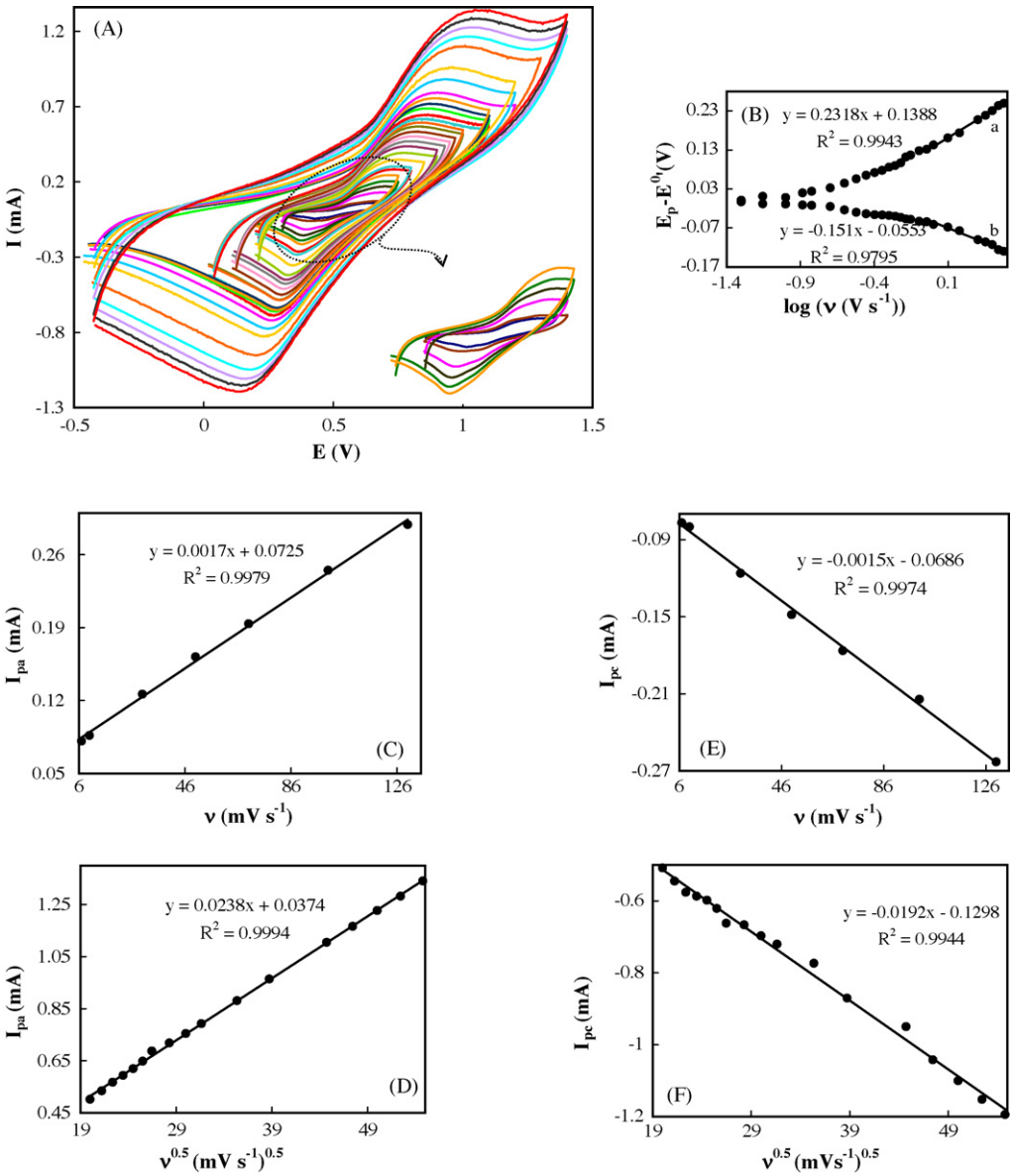

Fig. 1. (A) Cyclic voltammograms of ns-Ni-CC/Nf electrode in 100 mM NaOH solution recorded at potential sweep rates from the inner to the outer of 7, 10, 30, 50, 70, 100, 130, 150, 200, 250, 300, 350, 400, 450, 500, 550, 600, 650, 700, 800, 900, 1000, 1250, 1500, 2000, 2250, 2500, 2750 and 3000 mV s^{-1}. (B) Plot of $(E_p - E^{0\prime})$ with respect to the log ν. (C–E) Dependency of anodic (C) and cathodic (E) peak currents on the potential sweep rate at low values of 7–130 mV s^{-1} and dependency of anodic (D) and cathodic (F) peak currents on the square root of the potential sweep rate at high values of 400–3000 mV s^{-1}.

immobilized at the nanocomposite surface via the following reaction (Hajjizadeh et al., 2008; Heli et al., 2009b):

$$NiOOH + H_2O + e \leftrightarrows Ni(OH)_2 + OH^- \quad (1)$$

The peak-to-peak potential separation in the voltammograms deviated from the theoretical value of zero and increased at higher potential sweep rates. This result indicates a limitation in the charge-transfer kinetics, which is due to: (a) chemical interactions between the electrolyte ions and the modifier film, (b) dominance of electrostatic factors, (c) the lateral interactions of the redox couples present on the surface and/or (d) non-equivalent sites present in the film.

Laviron derived general expressions for the potential sweep voltammetric response of surface-confined electroreactive species (Laviron, 1979). The expressions for peak-to-peak potential separations $(\Delta E_p) > 200/n$ mV, where n is the number of exchanged electrons, are as follows:

$$E_{pa} = E^{0\prime} + X \ln\left[\frac{1-\alpha_s}{m}\right] \quad (2)$$

$$E_{pc} = E^{0\prime} + Y \ln\left[\frac{1-\alpha_s}{m}\right] \quad (3)$$

$$\ln k_s = \alpha_s \ln(1-\alpha_s) + (1-\alpha_s)\ln\alpha_s - \ln\left(\frac{RT}{nF\nu}\right) - \alpha_s\frac{(1-\alpha_s)nF\Delta E_p}{RT} \quad (4)$$

where $X = RT/(1-\alpha)nF$, $Y = RT/\alpha nF$, $m = (RT/F)(k_s/n\nu)$, E_{pa} and E_{pc} are the anodic and cathodic peak potentials, respectively, and α_s, k_s and ν are the electron-transfer coefficient, apparent charge-transfer rate constant and potential sweep rate, respectively. From these expressions, α_s can be determined by measuring the variation of the peak potential with respect to the potential sweep rate, and k_s

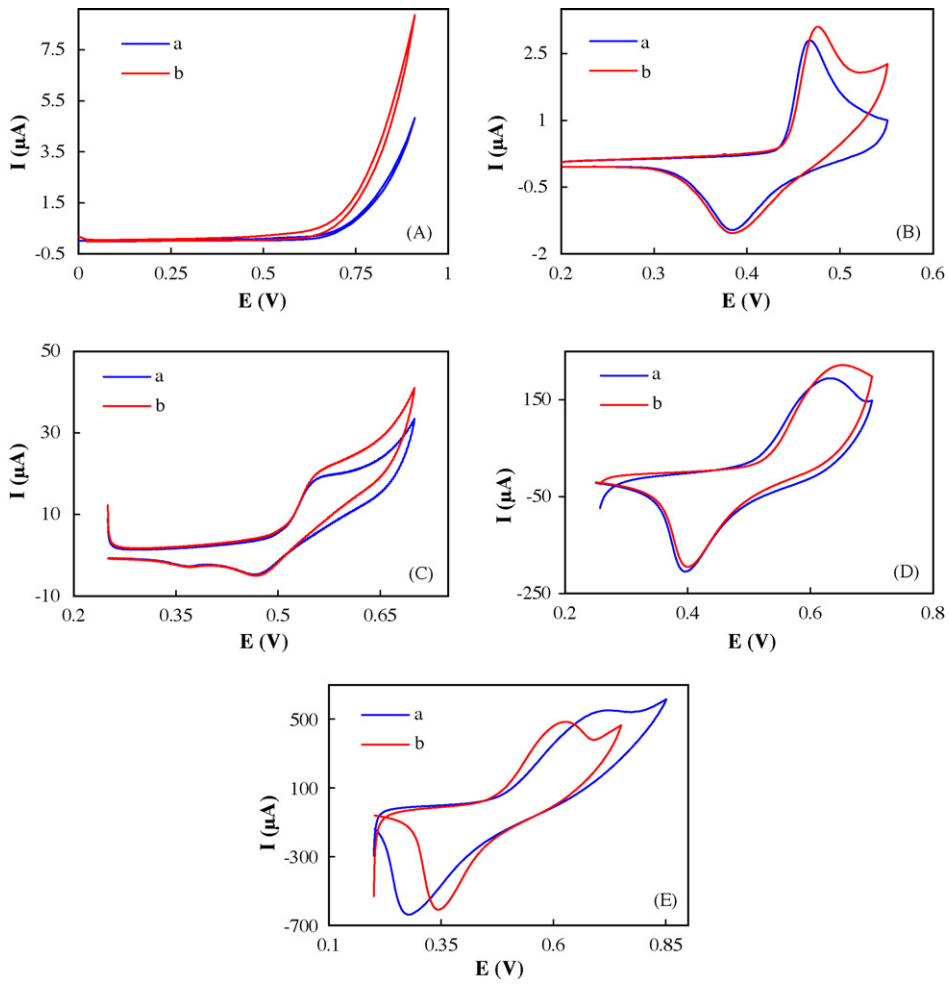

Fig. 2. Cyclic voltammograms of u-CPE (A), m-Ni-CC (B), n-Ni-CC (C), Zn@Ni-CC (D) and ns-Ni-CC (E) in the absence (curves a) and presence (curves b) of 1 mM ACh in 100 mM NaOH solution. The potential sweep rate was 25 mV s^{-1}.

can be determined by measuring the ΔE_p values. Fig. 1B shows the plot of $(E_p - E^{0\prime})$ with respect to the log ν for the anodic and cathodic peaks (the data was acquired from the cyclic voltammograms represented in Fig. 1A). It can be observed that for potential sweep rates of 1250–3000 mV s^{-1}, the values of $(E_p - E^{0\prime})$ are proportional to the logarithm of the potential sweep rate indicated by Laviron. Using the plot and Eqs. (2) and (4), the value of $\alpha_{s,a}$ (anodic electron-transfer coefficient) was determined as 0.74. In addition, using the plot and Eqs. (3) and (4), the value of $\alpha_{s,c}$ (cathodic electron-transfer coefficient) was determined as 0.37. This discrepancy suggests that the rate-limiting steps for the reduction and oxidation processes might not be the same (Luo et al., 2001). Moreover, the mean value of k_s was obtained as 4.64 s^{-1}. This value is higher than those reported elsewhere in the literature (Hajjizadeh et al., 2008; Berchmans et al., 1995) for the redox process of nickel species. This result indicates that the nanoshells of hollow nickel microspheres represent a higher electron-transfer rate in the redox process of nickel species in alkaline solution compared to the microstructures represented in Refs. (Hajjizadeh, 2008; Berchmans et al., 1995). In the voltammograms represented in Fig. 1A, the anodic and cathodic peak currents are proportional to the potential sweep rate at low values of 7–130 mV s^{-1} (Fig. 1C and E). This result is attributable to the electrochemical activity of an immobilized redox couple at the surface. From the slopes of these lines and using (Bard and Faulkner, 2001),

$$I_p = \left(\frac{n^2F^2}{4RT}\right)\nu A\Gamma_* \quad (5)$$

where I_p is the peak current, A is the electrode surface area and $\Gamma^*$is the surface coverage of the redox species and taking the average of both cathodic and anodic currents, a total surface coverage of the nanocomposite of about 1.702×10^{-8} mol cm^{-2} was derived. In the higher range of potential sweep rates of 400–3000 mV s^{-1} (Fig. 1D and F), the dependencies of the anodic and cathodic peak currents on the potential sweep rate are of square-root form, signifying the dominance of a diffusion process as the rate-limiting step in the total redox transition of the nanocomposite. This limiting-diffusion process, which was also reported for other Ni-based electrodes (Heli et al., 2009b; Roslonek and Taraszewska, 1994), may be due to the charge neutralization of the nanocomposite during the oxidation/reduction process.

3.3. Electrocatalytic oxidation of ACh on different composites

In an electrocatalytic reaction based on surface-confined mediation electron transfer, the electrocatalytic efficiency depends on both kinetics of charge-transfer process of the redox mediator, and

catalytic rate constant of the chemical reaction occurred between the mediator and the substrate (Heli et al., 2009a; Hajjizadeh et al., 2008). On the other hand, it is well known that the overall reactivity of an electrocatalyst can be size- and shape-dependent (Heli et al., 2009a,c, 2010a). In this regard, although the nickel-based composites showed similar signature in the cyclic voltammograms (vide infra, Fig. 2) and the voltammograms represented here are similar to those reported for other nickel-based electrodes (Hajjizadeh et al., 2008; Heli et al., 2009b; Berchmans et al., 1995), the electrocatalytic reactivities of different composites toward the electrooxidation processes can be size- and shape-dependent. Therefore, the effect of particle size and shape of the active catalyst (nickel oxyhydroxide species) in the course of anodic oxidation of ACh was studied. Fig. 2 shows cyclic voltammograms of u-CPE (A), m-Ni-CC (B), n-Ni-CC (C), Zn@Ni-CC (D) and ns-Ni-CC (E) in the absence (curves a) and presence (curves b) of 1 mM ACh in 100 mM NaOH solution. ACh represented very weak oxidation signal on u-CPE, while the nickel-based composites oxidized ACh with different efficiencies. All composites represented the typical cyclic voltammogram of nickel-based electrodes in alkaline solution in the absence of ACh (see also reaction (1)). The difference in the patterns of the voltammograms may be related to the rate of electron injection and/or ion intercalation into the nickel oxides generated during the potential sweeping. In the presence of ACh, the anodic peak currents in the all voltammograms increased, while the corresponding cathodic peak currents decreased or remained unchanged. From the cyclic voltammograms represented in Fig. 2, an electrocatalytic mechanism for the electrooxidation of ACh on the different nickel-based composites can be deduced in which the redox transition of the nickel species,

$$\mathrm{Ni(II)} \underset{k-1(E)}{\overset{k1(E)}{\rightleftarrows}} \mathrm{Ni(III)} + e \tag{6}$$

was followed by the oxidation of ACh via the following reaction:

$$\mathrm{Ni(III)} + \mathrm{ACh} \xrightarrow{k'} \mathrm{product} + \mathrm{Ni(II)} \tag{7}$$

From the data represented in Fig. 2, the anodic currents generated from different composites for the same concentration of ACh were measured and the corresponding catalytic efficiencies (CEs) were calculated as: $CE = (I_{ACh} - I_b)/I_b$, where CE is the catalytic efficiency, I_{ACh} is the current in the presence of ACh and I_b is the base current. The obtained values of CEs for different composites are summarized in Table 1. According to the results, u-CPE almost represented no electroreactivity toward the electrooxidation of ACh. n-Ni-CC represented a catalytic efficiency higher than m-Ni-CC. This means that the nanoparticles of nickel represented higher reactivity than those microparticles. It can be related to the small size of the particles which represent higher reactivity, i.e. nanosize effect (Narayanan and El-Sayed, 2003; Heli et al., 2009a,c, 2010a), because the currents were normalized for the effective surface areas of both composites. Zn@Ni-CC represented higher CE than both n-Ni-CC and m-Ni-CC. This may be related to the so-called strain and ligand effects of the core substrate on the shell compound (Sao-Joao et al., 2005; Stamenkovic et al., 2003). ns-Ni-CC represented the highest CE (between the composites which were constructed without Nafion). This means that nanoshells of nickel represented the highest reactivity towards the electrooxidation of ACh. This high reactivity can be related to oriented arrangement of nickel in the spheres' walls. These walls have high porosity (see Supplementary material S1) and the large degree of porosity of the hollow spheres could facilitate the diffusion of ACh into the porous structure. It should be also added that the non-normalized anodic currents with respect to the real surface area generated from ns-Ni-CC were very high, compared to the other composites (data not shown). This is due to the high surface area of the hollow sphere materials, compared to dense spheres of the similar size. The open hollow structure enables both the outer and inner surfaces of the material to come into contact with ACh, the empty core domain is able to accommodate larger number of ACh molecules, yield added benefits for the electrocatalytic process.

The effect of presence of Nafion in the composites was also investigated by cyclic voltammetry. Nafion can influence the current because Nafion and ACh are oppositely charged. In addition, Nafion can have an important rule on the selectivity of the electrochemical sensors (Heli et al., 2009a,d, 2010b) and are to be investigated shortly (vide infra). Cyclic voltammograms of ns-Ni-CC, ns-Ni-CC-Nf and ns-Ni-CC/Nf in the absence and presence of ACh were recorded (see Supplementary material S2). CEs for these composites were calculated and reported in Table 1. As it can be seen, when Nafion is present in the composite as a coated membrane, CE is the highest. Nafion as a negatively charged membrane, specially when it presents as a covering membrane and is exposed to the ACh solution, can adsorb and concentrate positively charged ACh species at the electrode surface. It causes the electrooxidation current to be enhanced near five times. The results indicate that ns-Ni-CC/Nf represents the highest electrocatalytic current and therefore, it was chosen for further studies and biosensing of ACh.

A steady-state current-potential curve was recorded for the electrocatalytic oxidation of ACh on ns-Ni-CC/Nf (see Supplementary material S3). Typical S-shaped plot was obtained and the transfer coefficient (α) was obtained by plotting the swept potential versus logarithm of the pseudo-steady-state current. The charge-transfer coefficient for the electrooxidation of ACh on the ns-Ni-CC/Nf surface was obtained as $\alpha = 0.41$. This indicates a near-symmetric barrier for potential energy change during the electrooxidation process with a slightly curvature to the reaction products.

Cyclic voltammograms of ns-Ni-CC/Nf in a wide range of potential sweep rates of 5–3000 mV s^{-1} in the presence of 3 mM ACh were recorded (see Supplementary material S4). Upon increasing the potential sweep rate, the anodic peak current increased and depended linearly on the square root of the potential sweep rate. This linear dependency indicates the domination of a diffusion-controlling step for the electrooxidation process. Based on this linear dependency, and using the Randles–Sevcik equation (Bard and Faulkner, 2001):

$$I_{pa} = (2.99 \times 10^5)\alpha^{1/2} n^{3/2} A C D^{1/2} \nu^{1/2} \tag{8}$$

where I_{pa} is the anodic peak current, A is the electrode surface area, D is the diffusion coefficient, and C is the bulk concentration of ACh, the diffusion coefficient of ACh was obtained to be 4.74×10^{-6} cm^2 s^{-1}. In addition, the value of the electron-transfer coefficient for the reaction can be obtained using the dependency of anodic peak potential on the natural logarithm of the potential sweep rate (Supplementary material S4), and from the equation (Harrison and Khan, 1970)

$$E_p = \left(\frac{RT}{2\alpha F}\right) \ln \nu + \text{constant} \tag{9}$$

which is valid for a totally irreversible diffusion-controlled process. Using this method, the electron-transfer coefficient for the electrooxidation of ACh on the ns-Ni-CC/Nf surface was obtained as 0.40. This value is in closed agreement with that obtained from Tafel plot (Supplementary material S3). Another point is that plotting the current function (peak current divided by the square root of the potential sweep rate) against the potential sweep rate revealed a negative slope (see Supplementary material S4). This further confirms the electrocatalytic nature of the processes.

3.4. Kinetics of electrocatalytic oxidation of ACh on ns-Ni-CC/Nf

Chronoamperometric studies were performed by setting the working electrode potentials to the desired values in order to measuring the catalytic rate constant of ACh electrooxidation on the ns-Ni-CC/Nf surface as well as diffusion coefficient of ACh. Chronoamperograms for ns-Ni-CC/Nf in the absence and presence of ACh over a concentration range of 0.001–9 mM were recorded (see Supplementary material S5). The applied potential step was 730 mV which would create a pure diffusional current. The transient current decayed in a Cotrellian manner, as the net currents varied linearly with the minus square roots of time. Therefore, a diffusion-controlled process is dominant for the electrooxidation of ACh; it was demonstrated previously using cyclic voltammetry (Supplementary material S4). Using the slope of the line, the diffusion coefficients of ACh can be obtained according to the Cottrell equation (Bard and Faulkner, 2001):

$$I = nFAD^{1/2}C\pi^{-1/2}t^{-1/2} \quad (10)$$

Using this method, the mean value of the diffusion coefficient of ACh was obtained as 4.62×10^{-6} cm^2 s^{-1}. This value is in agreement with that obtained using cyclic voltammetry and that reported in the literature (Heli et al., 2009a). Chronoamperometry can also be used to evaluate the catalytic rate constant according to (Bard and Faulkner, 2001):

$$\frac{I_{cat}}{I_L} = \gamma^{1/2}\left[\pi^{1/2}\mathrm{erf}(\gamma^{1/2}) + \exp\frac{(-\gamma)}{\gamma^{1/2}}\right] \quad (11)$$

where I_{cat} and I_L are the currents in the presence and absence of ACh, respectively, and $\gamma = k_{cat}Ct$ is the argument of the error function. k_{cat} is the catalytic rate constant, and t is elapsed time. In cases where $\gamma > 1.5$, erf($\gamma^{1/2}$) is almost equal to unity, and Eq. (11) can be reduced to:

$$\frac{I_{cat}}{I_L} = \gamma^{1/2}\pi^{1/2} = \pi^{1/2}(k_{cat}Ct)^{1/2} \quad (12)$$

From the slope of the I_{cat}/I_L versus $t^{1/2}$ plot, the mean values of k_{cat} obtained as 1.17×10^5 cm^3 mol^{-1} s^{-1}. This value is ≈2.7 times grater than that reported for the electrocatalytic oxidation of ACh on nanoparticles of copper (Heli et al., 2009a), is around three order of magnitude greater than reported for the electrocatalytic oxidation of carbohydrates on a nickel-polymer-modified electrode (Ojani et al., 2004) and is 30 and 1.4 times greater than obtained for the electrocatalytic oxidation of diclofenac and indomethacin, respectively, on nickel oxide-modified electrode (Hajjizadeh et al., 2007).

3.5. Biosensing of ACh

In order to develop a biosensing procedure for sensing and determination of ACh, the amperometry technique was employed. Typical amperometric signals obtained during successive increments of ACh to the solution using ns-Ni-CC, ns-Ni-CC-Nf and ns-Ni-CC/Nf, where a working potential of 670 mV was applied, are depicted in Fig. 3. The nanocomposite responses were proportional to the ACh concentration and ns-Ni-CC/Nf represented the highest sensitivity. The limits of detection (LOD) and quantitation (LOQ) of the procedure were calculated according to the 3SD/m and 10SD/m criteria, respectively, where SD is the standard deviation of the intercept and m is the slope of the calibration curves (Miller and Miller, 1994). The determined parameters for calibration curves of ACh using ns-Ni-CC/Nf were obtained as LOD = 49.33 nM, LOQ = 164.40 nM, RSD = 1.72%, bias = 1.34%, sensitivity = 48.58 ± 0.52 mA M^{-1} cm^{-2} and a linear range of 0.24–828 μM. A comparison between the sensing utility of some biosensors for ACh were also made (see Supplementary material S6). The present biosensor can determine ACh with a high sensitivity and a low limit of detection.

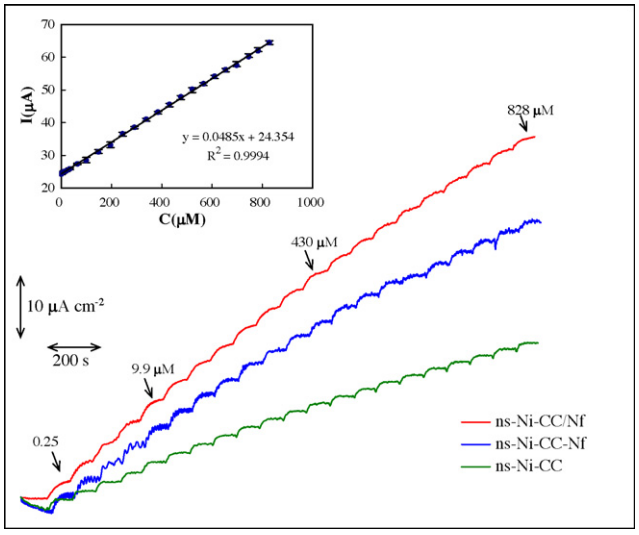

Fig. 3. Typical amperometric signals obtained during successive increments of ACh to 100 mM NaOH solution using ns-Ni-CC, ns-Ni-CC-Nf and ns-Ni-CC/Nf. The working potential was 670 mV. Inset: The calibration curve for ACh obtained using ns-Ni-CC/Nf.

3.6. Fouling resistance, stability and selectivity

In order to investigate the fouling resistance of the nanocomposite, consecutive cyclic voltammograms using ns-Ni-CC/Nf in 1 mM ACh solution were recorded (see Supplementary material S7). It was observed that the current as well as potential of the peak related to the ACh electrooxidation changed slightly (<4%) after 50 cyclic scans. This indicates that the intermediate and or product of the electrooxidation reaction did not adsorbed at the nanocomposite surface and the biosensor represents an antifouling behavior towards the ACh electrooxidation.

To verify the durability and long-term stability of the nanocomposite, consecutive cyclic voltammograms using ns-Ni-CC/Nf in 100 mM NaOH solution were recorded (see Supplementary material S8). It was found that the peak currents changed slightly (<5%) after 100 cyclic scans. In addition, the electrode was stored in 100 mM NaOH solution when not in use and retained its electroreactivity for 5 weeks. To verify the fabrication reproducibility of the biosensor, prepared under the same conditions, five ns-Ni-CC/Nf were fabricated and the amperometric responses of the nanocomposites in 1 mM ACh solution were measured. A RSD of 3.7% was obtained indicating that the fabrication method was highly reproducible.

In order to investigate the selectivity of the biosensor, the interference effects of some common biological interferences, L-ascorbic acid, dopamine, D-glucose, uric acid, L-cysteine, ephedrine and pseudoephedrine were tested (see Supplementary material S9). Under the experimental conditions applied in this work, no chemical interference was observed for all these compounds due to the rejection of the diffusion of these anionic compounds by Nafion membrane.

4. Conclusion

Different composites based on different size and shapes of the nickel catalysts were investigated in the course of the electrocatalytic oxidation of ACh. The nanocomposite comprised nanoshells of hollow nickel microspheres-carbon microparticles-

Nafion showed the highest performance for the process. ACh was oxidized on the nanocomposite via mediation of Ni(III) active species with an EC′ mechanism without any fouling of the surface. An amperometric procedure was successfully applied to the quantification of the ACh with high sensitivity. This remarkable electrocatalytic activity, stable response and selectivity of the nanocomposite are comparable with all other biosensors of ACh. The performance of the nanoshells of nickel-based nanocomposite indicates that it can be used as a sensitive amperometric detector for nanomolar detection of ACh.

Acknowledgment

We would like to thank the Research Councils of Islamic Azad University, Shiraz University of Medical Sciences and the Iran National Science Foundation (INSF) for supporting this research.

Appendix A. Supplementary data

Supplementary data associated with this article can be found, in the online version, at doi:10.1016/j.bios.2010.03.031.

References

Bard, A.J., Faulkner, L.R., 2001. Electrochemical Methods. New York, Wiley.
Barsoum, B.N., Watson, W.M., Mahdi, I.M., Khalid, E., 2004. J. Electroanal. Chem. 567, 277–281.
Berchmans, S., Gomathi, H., Rao, G.P., 1995. J. Electroanal. Chem. 394, 267–270.
Burmeister, J.J., Pomerleau, F., Huettl, P., Gash, C.R., Werner, C.E., Bruno, J.P., Gerhardt, G.A., 2008. Biosens. Bioelectron. 23, 1382–1389.
Davis, K., Berger, P.A.P., 1979. Brain Acetylcholine and Neuropsychiatric Disease. Plenum Press, New York.
Hajjizadeh, M., Jabbari, A., Heli, H., Moosavi-Movahedi, A.A., Haghgoo, S., 2007. Electrochim. Acta 53, 1766–1774.
Hajjizadeh, M., Jabbari, A., Heli, H., Moosavi-Movahedi, A.A., Shafiee, A., Karimian, K., 2008. Anal. Biochem. 373, 337–348.
Harrison, J.A., Khan, Z.A., 1970. J. Electroanal. Chem. 28, 131–138.
Heli, H., Hajjizadeh, M., Jabbari, A., Moosavi-Movahedi, A.A., 2009a. Biosens. Bioelectron. 24, 2328–2333.
Heli, H., Jabbari, A., Majdi, S., Mahjoub, M., Moosavi-Movahedi, A.A., Sheibani, S., 2009b. J. Solid State Electrochem. 13, 1951–1958.
Heli, H., Hajjizadeh, M., Jabbari, A., Moosavi-Movahedi, A.A., 2009c. Anal. Biochem. 388, 81–90.
Heli, H., Zarghan, M., Jabbari, A., Moosavi-Movahedi, A.A., 2009d. Sens. Actuators B 140, 245–251.
Heli, H., Majdi, S., Sattarahmady, N., 2010a. Sens. Actuators B 145, 185–193.
Heli, H., Zarghan, M., Jabbari, A., Parsaei, A., Moosavi-Movahedi, A.A., 2010b. J. Solid State Electrochem. 14, 787–795.
Jin, S.M., Yuan, L.S., Zhou, Y., Qiu, G.Z., Wan, C.F., 2006. Mater. Res. Bull. 41, 2130–2136.
John, B., Carolina, D., 2001. Medical Biochemistry. Mosby International, p. 497.
Laviron, E., 1979. J. Electroanal. Chem. 101, 19–28.
Lin, S., Chou, T.C., 2005. J. Electrochem. Soc. 152, H53–H57.
Luo, H., Shi, Z., Li, N., Gu, Z., Zhuang, Q., 2001. Anal. Chem. 73, 915–920.
Lou, X.W., Archer, L.A., Yang, Z., 2008. Adv. Mater. 20, 3987–4019.
Miller, J.C., Miller, J.N., 1994. Statistics for Analytical Chemistry, 4th ed. Ellis-Harwood, New York, p. 115.
Narayanan, R., El-Sayed, M.A., 2003. J. Phys. Chem. B 107, 12416–12424.
Ning, M., Zhu, H.F., Jia, Y.S., Niu, H.L., Wu, M.Z., Chen, Q.W., 2005. J. Mater. Sci. 40, 4411–4413.
Ojani, R., Raoof, J.B., Salmany-Afagh, P., 2004. J. Electroanal. Chemistry 571, 1–8.
Pepeu, G., Giovannini, M.G., 2004. Learn. Mem. 11, 21–27.
Roslonek, G., Taraszewska, J., 1994. Electrochim. Acta 39, 1887–1889.
Sao-Joao, S., Giorgio, S., Penisson, J.M., Chapon, C., Bourgeois, S., Henry, C., 2005. J. Phys. Chem. B 109, 342–347.
Shibli, S.M.A., Beenakumari, K.S., 2006. Electroanalysis 18, 465–470.
Shibli, S.M.A., Beenakumari, K.S., Suma, N.D., 2006. Biosens. Bioelectron. 22, 633–638.
Stamenkovic, V., Schmidt, T.J., Ross, P.N., Markovic, N.M., 2003. J. Electroanal. Chem. 554, 191–199.
Tsai, T.-H., 2000. J. Chromatogr. B 747, 111–122 (and references therein).
Woodman, T.F., Johnson, B., Marwaha, R.K., 1982. J. Liq. Chromatogr. Relat. Technol. 5, 1341–1348.